Influence of the state of stress on the brittle-ductile transition in granitic rock: Evidence from fault steps in the Sierra Nevada, California

Roland Bürgmann, David D. Pollard
Department of Geology, Stanford University, Stanford, California 94305-2115

ABSTRACT

Left-lateral strike-slip faults in the Lake Edison granodiorite (central Sierra Nevada, California) are composed of en echelon segments. Relative displacements across the faults apparently are transferred between segments by ductile shearing at right steps, and by extensional fracturing at left steps. The granodiorite within right steps displays mylonitic foliation, and thin sections show textures in quartz associated with dislocation glide, recovery processes, and dynamic recrystallization, whereas textures in feldspar are related to fracturing. Only centimetres outside the right steps, the rock fabric is approximately isotropic and deformation is accommodated by mineralized opening-mode fractures. The stress field calculated for the right-step geometry, when a boundary element model is used, shows an increase in mean compressive stress of up to 25 MPa within the step relative to that outside. This difference in stress apparently produced the contrasting behaviors of the granitic rock. Experimentally derived power-law flow laws do not predict these behaviors.

INTRODUCTION

The brittle-ductile transition zone is thought to exist at depths from 5 to 15 km, chiefly as a function of the crustal lithology, the geothermal gradient, and the lithostatic load. This is often idealized as the intersection of a pressure-dependent Coulomb failure law and a temperature-dependent creep law, but it probably involves a broad region of semibrittle behavior in which both brittle and crystal plastic processes occur.

We document a change from brittle to ductile deformation over distances as short as 1 cm from deformation mechanisms observed on metre-scale discontinuities along strike-slip faults in the Sierra Nevada (Fig. 1). An analysis of the microstructural fabrics within and outside of compressional fault steps, in combination with models of the associated stress field, shows the influence of the state of stress on the ductile yield strength in this natural example.

FAULT ZONES IN THE MT. ABBOTT QUADRANGLE: PREVIOUS WORK

In the medium- to fine-grained biotite-hornblende granodiorite of Lake Edison (Stern et al., 1981; Fig. 1), an episode of extensional fracturing resulted in joints filled with epidote, chlorite, and other hydrothermal constituents soon after the emplacement of the Late Cretaceous pluton (Segall and Pollard, 1983a). Left-lateral strike-slip faulting subsequently (75–79 Ma) nucleated on these mineral-filled planes of weakness (Segall and Pollard, 1983b; Segall et al., 1990). Estimates of temperature and pressure for the faulting event are 300–350 °C and 100–200 MPa, respectively, based on microstructural evidence and the inferred crystallization pressures in the area (Martel et al., 1988; Ague and Brimhall, 1988). Offsets along the faulted joints are in the range of centimetres to 2 m, and fault segments range from a few metres to several tens of metres in length.

Conditions during faulting were close to the brittle-ductile transition (Segall and Simpson, 1986). Extensional brittle fracturing accompanied faulting, as evidenced by oblique mineralized opening-mode fractures (splay cracks) at fault ends and within left steps of overlapping en echelon fault segments. Mylonitic fabrics in the granodiorite are mostly localized within right steps (Fig. 1, B and C).

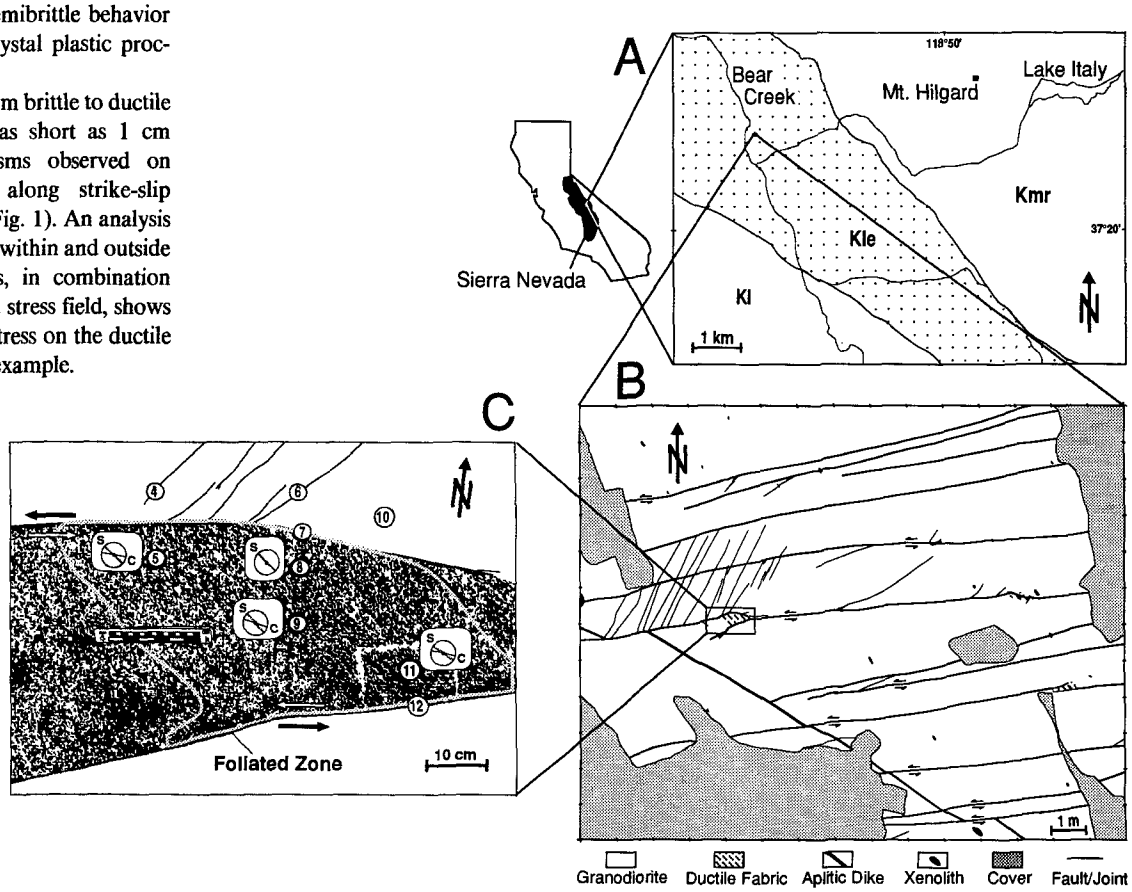

Figure 1. A: Map of Bear Creek region of Mt. Abbot quadrangle. Heavy lines indicate pluton contacts. Kl—Lamarck granodiorite, Kle—granodiorite of Lake Edison, Kmr—quartz monzonite of Mono Recesses. B: Outcrop map of faults, fractures, and right steps. C: Detailed map of step analyzed here. Fabric orientations (S and C planes) from four cores are indicated in boxed diagrams. Circled numbers indicate locations of cored samples.

A few faults show evidence for distributed mylonitic textures up to about 50 cm away from the faults. Segall and Simpson (1986) argued that hydrothermal fluid flow in the early dilatant joints led to an increased concentration of water and consequent "reaction softening" or hydrolytic weakening (Griggs and Blacic, 1965) in the wall rock. Kronenberg et al. (1990) showed that water concentrations in quartz were indeed highest in the central part of a sheared zone that formed about a transpressional fault segment. Water is surely important in the deformation of the granodiorite, which shows abundant evidence for hydrothermal alteration, high fluid pressure, and dissolution processes. However, upon examination of the fault steps, it is clear that the foliation is not distributed evenly around the faults, but is present only within right steps. As we will show here, this indicates that a change in the state of stress was required to cross the brittle-ductile transition.

DEFORMATION ASSOCIATED WITH FAULT STEPS

Whereas deformation within left steps is accommodated by extensional jointing and fractures, the right steps display S-C mylonitic fabrics (Lister and Snoke, 1984) indicating a component of noncoaxial flow. Distinct shear surfaces (C planes), rich in fine-grained mica and finely recrystallized quartz, separate zones of mostly undeformed feldspars and plastically deformed quartz and mica. The latter show a preferred grain orientation (S planes), oblique to the shears and the step-bounding faults, that defines the observed foliation. Foliation is oriented at angles of 25° to 35° close to the faults and shows higher angles of 40° to 55° in the center of the fault steps, whereas the C planes deviate from the fault strike by up to 15°, also in a clockwise sense (Fig. 1C).

Figure 2A (from core 5 in Fig. 1C) shows the typical microstructures developed in the ductilely deformed granodiorite in the right steps. Quartz is dynamically recrystallized, and there is a strong preferred orientation of the new grains. Biotite (commonly altered to chlorite) has been plastically deformed and shows typical "mica fish" structures (Lister and Snoke, 1984). Feldspar grains underwent extensional cracking, shear fracturing along cleavage planes, and cataclastic flow at grain boundaries. Patchy undulatory extinction in some feldspar grains is interpreted to be due to submicroscopic cataclasis (Tullis and Yund, 1987). Myrmekites commonly are found crushed and have undergone significant deformation through cataclastic flow of the feldspar constituent in a matrix of fine-grained quartz. Overall, deformation is semibrittle, dominated by flow of a crystal plastically deforming matrix of quartz and mica enveloping rigid grains of feldspar, hornblende, and opaques.

Only millimetres away from the mylonites, the rock outside of the right steps shows no evidence of significant ductile straining. Extensional, mineral-filled fractures oriented oblique to the faults accommodate some deformation outside of the steps, but the magnitude of strain is significantly lower than that accommodated by flow within the steps. Approximately 60 opening-mode fractures northwest of the fault step shown in Figure 1B accommodate about 2% extension. Figure 2B (from core 4 in Fig. 1C) shows an extensional fracture breaking the approximately isotropic granodiorite. Quartz exhibits undulatory extinction, but we see no evidence for recrystallization. Grain-scale shear and opening mode fractures are common in feldspars, and cracks are filled with fine-grained quartz and chlorite.

STRESS FIELD ASSOCIATED WITH FAULT STEPS

To gain a better understanding of the rheology of granitic rock as a function of the state of stress, we numerically calculated the stress field about the right steps using DIS3D (Erikson, 1987). Structural observations from one of the fault steps (Fig. 1) were used to define the geometric parameters of the model. The stress field in an elastic, isotropic, and homogeneous body was computed by using a model involving a series of 88 rectangular displacement-discontinuity surfaces that were combined to represent two left-lateral 20-m-long faults (overlap = 40 cm, step width = 25 cm) with an elliptical slip distribution. Prescribed displacement discontinuities of several millimetres on the surfaces are imposed as boundary conditions of the model. Then the stress perturbations due to fault slippage are superimposed with a uniform remote stress field, where the maximum and the least principal stresses (σ_1, σ_3) are horizontal (i.e., a strike-slip environment). A steady-state situation is envisioned in which relaxation processes (plastic strain, fracture, and diffusive mass transfer) keep pace with the faulting-induced stress changes. However, the time-dependent deformation and inelastic strain development cannot be addressed with this simple elastic model.

Using a forward-modeling approach, we compute a stress field that satisfies constraints derived from the field observations. Two structures—splay cracks and fabric—are used to correlate to local stress orientations. Splay cracks outside of the step strike about 50° oblique to the faults. We assume that these cracks are oriented parallel to the maximum principal stress σ_1, because no shear offsets occurred along them. For splay cracks to form, the effective tensile stress, σ_3 (eff) must have been larger than the tensile strength of the rock. Shear surfaces (C planes) within the plastically deformed mylonite of the right steps are inferred to be oriented at an angle of between 30° and 45° to the local σ_1. Elongated mineral grains that define the foliation (S planes) are thought to indicate the direction of the long axis of the finite strain ellipse (Ramsay, 1980). The angle between S and C surfaces varies from about 30° to 40° across the fault step, suggesting that σ_1 is oriented approximately perpendicular to the foliation. Some rotation of the S and C orientations may occur as finite strain develops, but, in light of the observed shear-strain magnitudes ($\gamma < 1$), the difference between the estimated and true stress directions is thought to be less than 10°. Remote mean stress ($P = [\sigma_1 + \sigma_2 + \sigma_3]/3$) is assumed to be 100 MPa. The larger the imposed offset on the faults, the greater the remote maximum shear stress ($[\sigma_1 - \sigma_3]/2$) for the model results to be consistent with the inferred principal stress directions. At lower remote shear stresses, the model predicts approximately fault-parallel shortening in the right step, not the strongly oblique orientations observed.

Figure 3A shows contours of the local mean

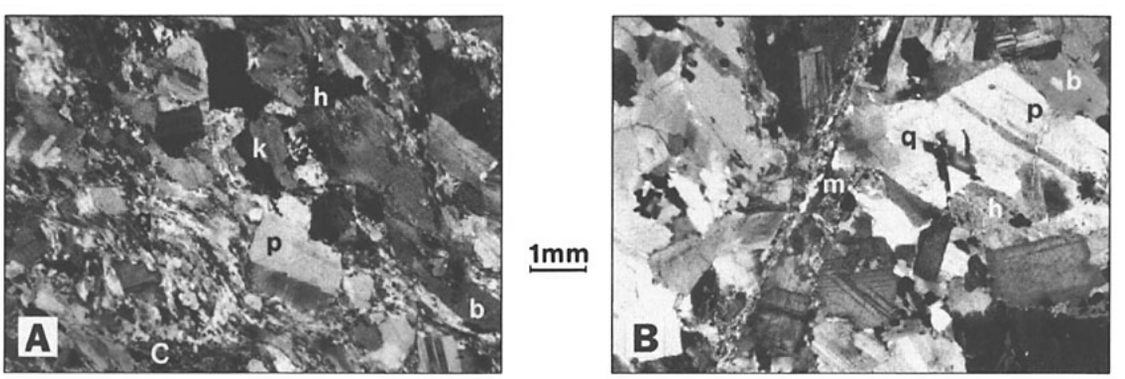

Figure 2. Photo micrographs of thin sections under crossed nicols. A: Core 5 (Fig. 1C) from ductilely deformed step showing recrystallized quartz, fractured feldspars, and fabrics related to noncoaxial flow. B: Core 4, located 10 cm away from core 5, shows brittle fractures and no fabric development. C—mylonitic C surface, b—biotite, h—hornblende, k—potassium feldspar, m—myrmekite, p—plagioclase, q—quartz.

stress and the orientation of the principal stresses assuming 2 mm of fault slip and a remote shear stress of 25 MPa. Mean stress increases of 10 to 25 MPa are calculated for the area within the fault step. The shaded regions in Figure 3A are areas where the least principal stress falls below 70 MPa, indicating areas where tensile fractures might form, given fluid pressure in excess of this figure.

Magnitudes of the local maximum shear stress are elevated around the fault tips and within the fault step as shown by contours in the lower left part of Figure 3B. An Arrhenius-type creep law (see Discussion) predicts higher strain rates in these regions. The predicted strain rates, contoured in the upper right part of Figure 3B, were calculated from the computed shear stresses (assuming T = 350 °C) by using the power-law parameters derived experimentally for wet Westerly granite (Hansen and Carter, 1982).

We postulate that mylonitic fabrics should develop first in areas of greatest shear strain rates. Contrary to the predicted strain-rate field in Figure 3B, we observe no mylonitic fabrics outside the fault steps. However, the area outlined by elevated mean-stress magnitudes in Figure 3A does correlate well with that of the mylonitic fabrics.

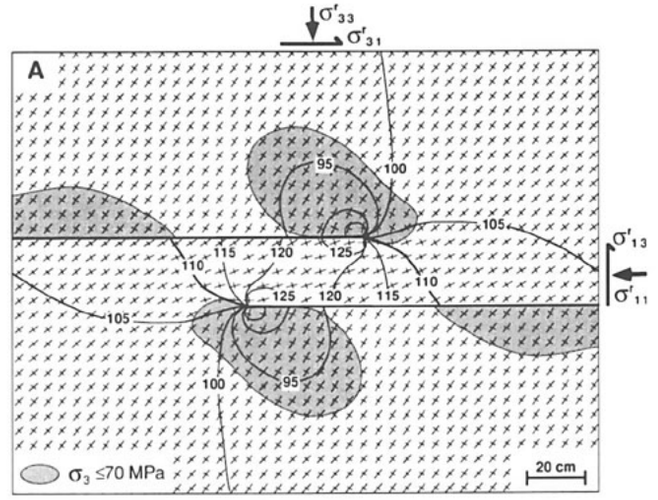

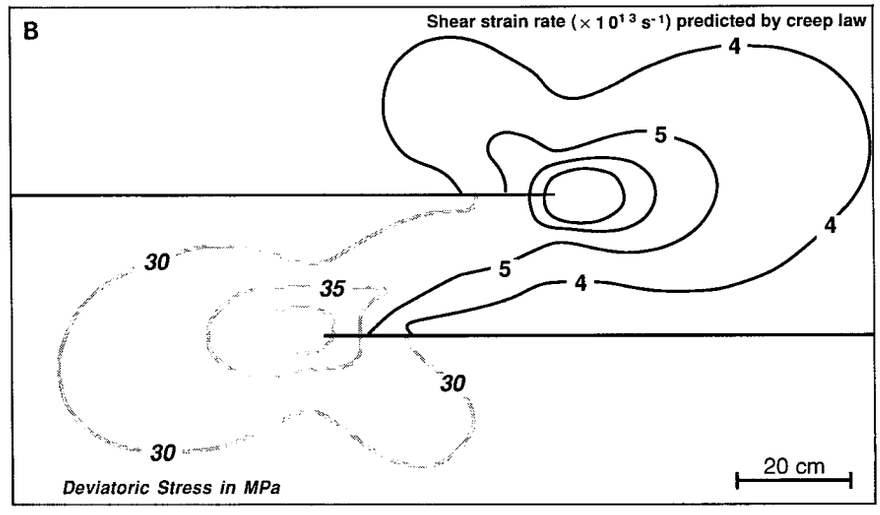

Figure 3. A: Mean-stress distribution and trajectories of principal stress directions near right step. Maximum slip on two faults was 2 mm at center of fault segments, diminishing toward fault ends in elliptical distribution. B: Contours of maximum shear-stress magnitudes (lower left) and shear strain rates predicted by power-law creep law (upper right).

DISCUSSION

The major factors influencing the active deformation mechanisms in granitic rocks are the mineral composition and structure, strain rate, temperature, fluids, and state of stress (Tullis, 1990). Over distances of a few centimetres across the step-bounding faults in the Mt. Abbot quadrangle, the lithology, temperature, and fluid compositions and concentrations probably do not vary so abruptly as to play a significant role in the drastic change in deformation. Yet the mean-stress field should have a sharp discontinuity across the faults (Fig. 3A). This suggests that the different state of stress is the important variable.

There is some experimental evidence on the effects of the stress state on the rheological behavior and strength of rock under dry conditions and in the presence of fluids. At low temperatures, the tensile strength can be several orders of magnitude lower than the compressive strength at high confining pressures (Scholz, 1990). At higher temperatures, when the flow stress is less strongly influenced by the confining pressure, experimenters infer that crystal plasticity, a constant-volume process, is the dominant mechanism of deformation. However, to attain crystal plastic behavior in rocks at high temperatures, it is necessary to apply some confining pressure (Paterson, 1978). Increased confining pressure may be needed (1) to offset the anisotropic thermal expansion of individual mineral grains (Paterson, 1978), (2) to inhibit fracturing by increasing crack-normal stresses (Paterson, 1978), and (3) to enhance the hydrolytic weakening effect seen in experiments (Tullis and Yund, 1989). The immediate effect of introducing fluids is to enhance fracture, both by lowering the effective crack-normal stresses and through stress corrosion, but at higher pressures and temperatures the net effect is a lowering of the temperature of the transition from microcracking (cataclasis) to dislocation glide and climb by about 150–200 °C for both quartz and feldspar (Tullis et al., 1979).

The stresses required for brittle fracture and for plastic flow are shown on a deformation-mechanism map in principal-stress space in Figure 4 (Hallam and Ashby, 1990). (See Scholz [1990] for a discussion of the failure laws and the choice of parameters used here.) The shaded and dashed lines in Figure 4 indicate a tensile fracture criterion ($\sigma_3 - P_p = -T_0$) and a compressional, Coulomb-type, failure law ($\tau = \tau_0 + \mu\,[\sigma_n - P_p]$), respectively; where P_p is the pore fluid pressure, T_0 is the tensile strength (here 5 MPa), τ_0 is a cohesive term (here 10 MPa), μ is the coefficient of internal friction (here 0.75), and τ and σ_n are the shear and normal stresses resolved on a plane. Under the assumption that the pore pressure is 70% of the lithostatic load of 100 MPa, the region defined by $\sigma_3 \leq (P_p - T_0)$ = 65 MPa represents stress states at which we expect tensile fractures to accommodate most of the deformation. The compressional failure law expressed in terms of the principal stresses is σ_1 = 1.44 σ_3 + 19.5 MPa at the postulated pore pressure.

Thick diagonal lines in Figure 4 show an experimentally derived flow law of the form $\dot{\epsilon} = A \cdot (\sigma_1 - \sigma_3)^n \cdot e^{(-\Delta H/RT)}$ at temperatures of 300 and 350 °C and strain rates ($\dot{\epsilon}$) ranging from 10^{-14} to 10^{-12} s^{-1}, using the material constants (A, ΔH, and n) for wet Westerly granite from Hansen and Carter (1982). In this equation R is the universal gas constant and T is temperature in kelvins. The flow law is of the form $\sigma_1 = \sigma_3$ + constant, indicated by straight lines at 45° to the coordinate axes on the σ_1 vs. σ_3 plot. Where the two brittle failure laws intersect the creep law, a transition from brittle to ductile deformation at a given strain rate is expected to take place.

We can now locate the computed stress states of the numerical model on the deformation-mechanism map in principal-stress space as indicated by the arrows labeled 1, 2, and 3 in Figure 4. The occurrence of tensile fracturing

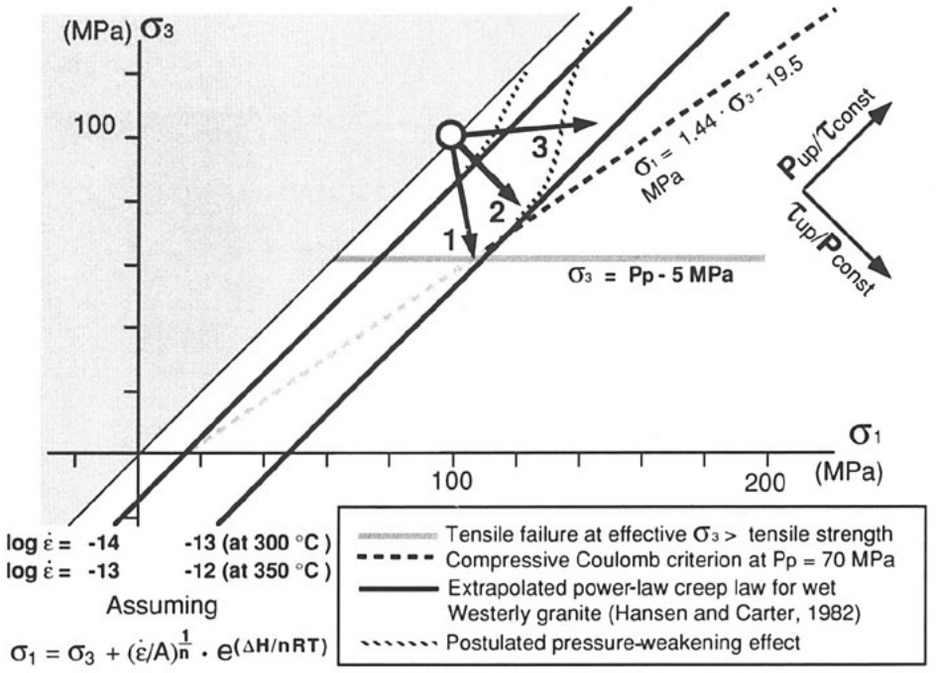

Figure 4. Deformation-mechanism map in principal-stress space based on brittle and ductile deformation laws in strike-slip environment ($\sigma_2 = [\sigma_1 + \sigma_3]/2$ is vertical). If pore pressure exceeds least principal stress by more than tensile strength (~5 MPa), tensile failure is predicted. Coulomb-Navier criteria delineates area where brittle failure is to be expected, and flow-law lines indicate stress states at which ductile flow (at strain rates ranging from 10^{-14} to 10^{-12} s^{-1}) occurs in wet Westerly granite at 300 and 350 °C (Hansen and Carter, 1982). Pressure-weakening effect is schematically drawn as deviation from (inherently pressure independent) power-law flow law, leading to lower strength and increased strain rates at elevated pressures. Starting out from confining pressure of 100 MPa at pore pressure of 70 MPa, response of granitic rock under different loading conditions encountered around Sierran fault steps can be considered. As we change shear stress τ and/or confining pressure P to values predicted in model, different deformation processes will dominate. This is schematically illustrated by three arrows indicating stress states in zones of (1) splay cracks, (2) undeformed rock away from faults, and (3) right steps.

adjacent to the Sierra Nevadan fault steps indicates that the effective least principal stress ($\sigma_3 - P_p$) exceeded the tensile strength of the rock, leading to brittle fracturing. In our numerical fault-step model, the least principal stress in the region of tension cracks is <70 MPa (Fig. 3A), indicating that fluid pressures may have been as high as 75 MPa, if a tensile strength of 5 MPa is assumed. A dependence of the flow strength on the mean stress has been described in the previous section. This pressure-dependent (hydrolytic?) weakening effect is indicated in schematic form in Figure 4 by a dashed-line deviation from the straight power-law flow law at higher pressures.

CONCLUSIONS

Field observations along faults in the Sierra Nevada, in combination with numerical modeling of the stress fields about en echelon fault steps, illustrate the effects of the stress state on the brittle and/or crystal plastic deformation of granitic rock. Increased mean stresses (10 to 25 MPa) within the fault steps allow the accommodation of large strains by plastic deformation mechanisms in quartz and mica. The pressure-weakening effect is possibly due to the pressure dependence of hydrolytic weakening in quartz. Thus, at a given temperature, rocks in zones of fluid infiltration *and* high mean stress will be weaker and will show a greater proportion of dislocation glide and climb. Tensile effective least principal stresses adjacent to the fault steps promote tensile fracturing. The strength of a rock and the acting deformation mechanisms vary significantly depending on the sign of the effective least principal stress and the magnitude of the confining pressure.

REFERENCES CITED

Ague, J.J., and Brimhall, G.H., 1988, Magmatic arc asymmetry and distribution of anomalous plutonic belts in the batholiths of California: Effects of assimilation, crustal thickness, and depth of crystallization: Geological Society of America Bulletin, v. 100, p. 912–927.

Erikson, L.L., 1987, DIS3D: A three dimensional dislocation program with applications to faulting in the earth [M.S. thesis]: Stanford, California, Stanford University, 167 p.

Griggs, D.T., and Blacic, J.D., 1965, Quartz: Anomalous weakness of synthetic crystals: Science, v. 147, p. 292–295.

Hallam, S.D., and Ashby, M.F., 1990, Compressive brittle fracture and the construction of multi-axial failure maps, *in* Barber, D.J., and Meredith, P.G., eds., Deformation processes in minerals, ceramics and rocks: London, Unwin Hyman, p. 84–108.

Hansen, F.D., and Carter, N.L., 1982, Creep of selected crustal rocks at 1000 MPa: Eos (Transactions, American Geophysical Union), v. 63, p. 437.

Kronenberg, A.K., Segall, P., and Wolf, G.H., 1990, Hydrolytic weakening and penetrative deformation within a natural shear zone, *in* Duba, A.G., ed., The brittle-ductile transition in rocks: American Geophysical Union Monograph 56, p. 21–36.

Lister, G.S., and Snoke, A.W., 1984, S-C mylonites: Journal of Structural Geology, v. 6, p. 617–638.

Martel, S.J., Pollard, D.D., and Segall, P., 1988, Development of simple strike-slip fault zones in granitic rock, Mount Abbot quadrangle, Sierra Nevada, California: Geological Society of America Bulletin, v. 100, p. 1451–1465.

Paterson, M.S., 1978, Experimental rock deformation—The brittle field: Berlin, Springer-Verlag, 254 p.

Ramsay, J.G., 1980, Shear zone geometry: A review: Journal of Structural Geology, v. 2, p. 83–99.

Scholz, C.H., 1990, The mechanics of earthquakes and faulting: Cambridge, England, Cambridge University Press, 439 p.

Segall, P., and Pollard, D.D., 1983a, Joint formation in granitic rock of the Sierra Nevada: Geological Society of America Bulletin, v. 94, p. 563–575.

——1983b, Nucleation and growth of strike-slip faults in granite: Journal of Geophysical Research, v. 88, p. 555–568.

Segall, P., and Simpson, C., 1986, Nucleation of ductile shear zones on dilatant fractures: Geology, v. 14, p. 56–59.

Segall, P., McKee E.H., Martel, S.J., and Turrin, B.D., 1990, Late Cretaceous age of fractures in the Sierra Nevada batholith, California: Geology, v. 18, p. 1248–1251.

Stern, T.W., Bateman, P.C., Morgan, B.A., Newall, M.F., and Peck, D.L., 1981, Isotopic U-Pb ages of zircon from the granitoids of the central Sierra Nevada, California: U.S. Geological Survey Professional Paper 1185, 17 p.

Tullis, J.A., 1990, Experimental studies of deformation mechanisms and microstructures in quartzo-feldspathic rocks, *in* Barber, D.J., and Meredith, P.G., eds., Deformation processes in minerals, ceramics and rocks: London, Unwin Hyman, p. 190–227.

Tullis, J.A., and Yund, R.A., 1987, Transition from cataclastic flow to dislocation creep of feldspar: Mechanisms and microstructures: Geology, v. 15, p. 606–609.

——1989, Hydrolytic weakening of quartz aggregates: The effects of water and pressure on recovery: Geophysical Research Letters, v. 16, p. 1343–1346.

Tullis, J.A., Shelton, G.L., and Yund, R.A., 1979, Pressure dependences of rock strength: Implications for hydrolytic weakening: Bulletin Minéralogique, v. 102, p. 110–114.

ACKNOWLEDGMENTS

Supported by the Geological Society of America, Sigma Xi, the McGee research fund, and the Rock Fracture Project. Ramón Arrowsmith, Peter Christiansen, Steve Martel, Michael Pollard, and Betty Suh helped with the field work. We thank Jan Tullis and Ben van der Pluijm for helpful reviews.

Manuscript received November 25, 1991
Revised manuscript received April 2, 1992
Manuscript accepted April 6, 1992